Simulation on Solar Type II Radio Bursts associated with Coronal Mass Ejections

Laboratory for Plasma Astrophysics, Faculty of Engineering
J.I.Sakai, T.Mori and S.Saito
m042274@ems.toyama-u.ac.jp

The wave emission process of solar Type II radio bursts associated with Coronal Mass Ejections (CME) is investigated by using two dimensional, electromagnetic, relativistic Particle-In-Cell (PIC) code. Two simulation results are shown: the first case is that the CME propagates perpendicular to the local magnetic field, and the second case is that the CME propagates obliquely to the local magnetic field where only the case of the propagation angle of 80 degree is shown. It is shown that fast magnetosonic shock wave is formed with both protons and electrons accelerated by the surfatron acceleration mechanism. It is also shown from the first case that near the shock front the electron Bernstein waves are generated and they can be converted to the extra-ordinary electromagnetic waves (Type II radio bursts) through the direct linear mode conversion. It is found from the second case that near the shock front the electrostatic Langmuir waves (Z-mode) are generated and they can be also converted to the extra-ordinary electromagnetic waves through the direct linear mode conversion.
Keywords : Sun: radio radiation Sun: Type II burst Sun: CME

1 Introduction

The origin of the shock waves in the solar corona that manifest themselves as solar Type II radio bursts is one of important subjects of solar and solar-terrestrial physics. Cliver et al. (1999) concluded that metric Type II bursts have their root cause in fast coronal mass ejections (CME). A general picture of emission from Type II shocks is thought such that the emission mechanism is plasma emission near the fundamental and second harmonic (Smith 1970; Melrose 1980). Langmuir waves are produced by beams produced in the shock. The excited Langmuir waves may be converted into escaping radio waves by nonlinear wave-wave processes (See for reviews, Goldman and Smith 1986; Cairns et al. 2003; Aschwanden 2004). Recent observations from the Ulysses spacecraft (Simnett 2003) have measured the energy spectrum of the ambient ions associated with the passage of a fast magnetosonic quasi-perpendicular shock driven by a CME. Near the shock front the energy spectrum of the accelerated ions, which are predominantly protons, exhibit features (maxima) at about 250 keV-1.5 MeV. Simnett, Sakai and Forsyth (2004) showed that the protons with an energy of about 1 MeV, which corresponds to $(m_i/m_e)V_A(M_A-1)^{3/2}$, can be accelerated by the surfatron mechanism of a fast magnetosonic shock wave propagating almost perpendicular to an ambient magnetic field. The in situ measurements therefore illustrate directly that this mechanism is very probably responsible for interplanetary particle acceleration. The shock is also accompanied by a increase in the near-relativistic electron intensity of almost two orders of magnitude.

In the present paper we address the formation of shock waves driven by CME, acceleration process of both protons and electrons and the emission mechanism of electromagnetic waves (solar Type II bursts) from the shock front, by using a two-dimensional, fully relativistic Particle-In-Cell (PIC) simulation. Two simulation results are shown: the first case is that the CME propagates perpendicular to the local magnetic field, and the second case is that the CME propagates obliquely to the local magnetic field where only the case of the propagation angle of 80 degree is shown. It is shown that fast magnetosonic shock wave is formed with both protons and electrons accelerated by the surfatron acceleration mechanism. It is also shown from the first case that near the shock front the electron Bernstein waves are generated and they can be converted to the electromagnetic waves (Type II radio bursts) through the direct linear mode conversion. It is found from the second case that near the shock front the electrostatic Langmuir waves (Z-mode) are generated and they can be also converted to the electromagnetic waves through the direct linear mode conversion.

The present letter is organized as follows. In §2 the simulation model and the parameters used in the simulations are presented. In §3 we show the simulation results. In §4 we summarize our results.

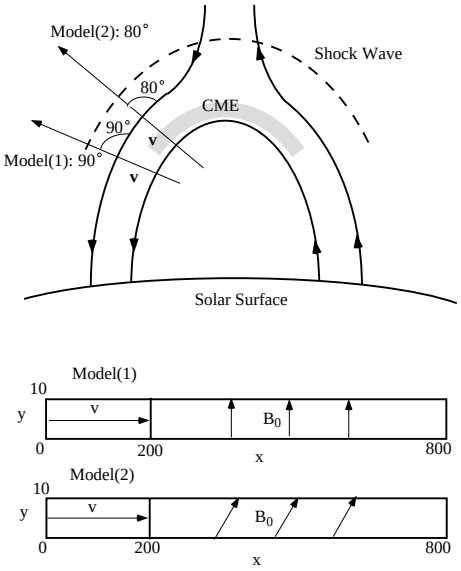

Figure 1: The upper figure shows a schematic picture of coronal mass ejections (CME) associated with a shock wave and two models: Model (1) is that the CME propagates perpendicular to a magnetic field, and Model (2) is that the CME propagates obliquely with angle of 80 degree to a magnetic field. The lower figures show the system size and coordinate system used in the simulation.

2 Simulation Model

In Fig.1 we present a schematic picture of coronal mass ejections (CME) associated with a shock wave. We consider two models: Model (1) is that the CME propagates perpendicular to a magnetic field, and Model (2) is that the CME propagates obliquely with angle of 80 degree to a magnetic field. The lower figures in Fig.1 show the system size and coordinate system used in the simulation.

We use 2D3V, the fully relativistic electromagnetic PIC code, modified from the 3D3V TRISTAN code (Buneman 1993). The system size is $L_x = 800\Delta$ and $L_y = 10\Delta$, where $\Delta(= 1.0)$ is grid size. The free boundary condition in the x direction, and the periodic boundary condition in the y direction are imposed on particles and fields. We divided the simulation domain into two areas: left side region ($x \leq 200\Delta$) and right side region ($x > 200\Delta$). In the left side region, the average number of electron-ion pairs is 400 per cell, initial flow velocity $v = 0.24c$ is applied to the x-direction by the electric field E_z through $E_z = v_x B_y$. This flow velocity is three times faster than Alfvén velocity $v_A = 0.08c$. In the right side region, there are 100 electron-ion pairs per cell. The external magnetic field $B_y = B_0$ is applied to y-direction, that is perpendicular to the flow direction.

The parameters used in this simulation are as follows. The ratio of ion mass to the electron mass is $m_i/m_e = 64$, the ratio of electron cyclotron frequency to the plasma frequency is about $\omega_{ce}/\omega_{pe} = 0.63$, plasma beta is $\beta = 0.05$, skin depth is $c/\omega_{pe} = 10.0\Delta$, electron thermal velocity is $v_{th,e} = 0.1c$, electron Larmor radius is $\rho_e = 1.58\Delta$, ion Larmor radius is $\rho_i = 12.7\Delta$, and the simulation time step is $\omega_{pe}\Delta t = 0.05$ respectively. The parameters ω_{ce}/ω_{pe}, β, c/ω_{pe}, $v_{th,e}$, ρ_e, and ρ_i are calculated in the right side region.

3 Simulation Results

In Figs.2 (c)-(h) we present summary of shock formation driven by the CME and the acceleration of both electrons and ions at $\omega_{pe}t = 90$. Fig.2(a) shows the electric field E_x that is initially absent in the system. Fig.2(b) show the initial magnetic field B_y perpendicular to the flow direction of the CME. As the time goes on, the fast magnetosonic shock wave with Alfvén Mach $M_A = 3$ is formed as seen in Fig.2(d). The fast magnetosonic shock is characterized with a strong electrostatic field E_x in the shock front as seen in Fig.2(c), that plays an important role for the particle acceleration through the surfatron mechanism (Ohsawa 1985; Sakai & Ohsawa 1987; Ohsawa & Sakai 1987). Behind the shock front, there appears also electrostatic field as seen in Fig.2(c) that is generated by the counter-streaming instability caused from the plasma particles reflected from the shock front. The Fig.2(e) and Fig.2(g) show the phase-space plots (V_x - x) for the ions and the electrons, respectively. As seen in Fig.2(e), some ions are reflected to both sides of the shock front. While, as seen in the electron phase-space plot of Fig.2(g), the reflected electrons behind the shock front mix up together with the in-coming electrons, because the counter-streaming instability occurs in the shock region. This is a reason why there appear the electrostatic waves behind the shock front as seen in Fig.2(c). We will investigate in details the nature of the electrostatic fields excited behind the shock front later.

We note here that both electrons and ions can be strongly accelerated in the z-direction near the shock front through the surfatron mechanism. Fig.2(f) and Fig.2(h) show the phase-space plots (v_z -x) of the ions and the electrons, respectively. The details of the acceleration process and the comparison with recent observations is discussed by Simnett et al.(2004). They showed that the observed proton acceleration agrees well with the theory as well as the simulation results of the surfatron mechanism. The

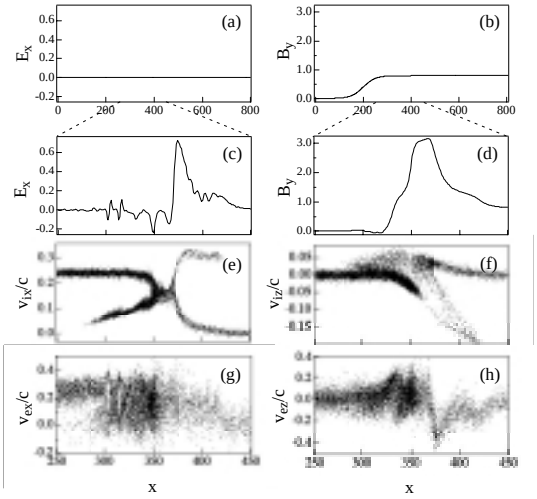

Figure 2: Simulation results for Model (2). (a) The electrostatic field E_x and (b) magnetic field B_y at $\omega_{pe}t = 0$. (c) The electrostatic field E_x and (d) magnetic field B_y at $\omega_{pe}t = 90$. (e) The ion phase space plot (v_{ix} - x) and (f) ion phase space plot (v_{iz} - x) at $\omega_{pe}t = 90$. (g) The electron phase space plot (v_{ex} - x) and (f) electron phase space plot (v_{ez} - x) at $\omega_{pe}t = 90$.

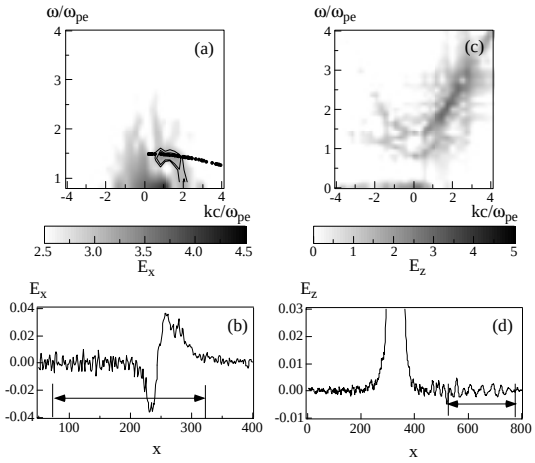

Figure 3: Simulation results for Model (1): (a) The dispersion relation for E_x obtained by space-time Fourier transformation ($70 \leq$ x ≤ 326, and $0 \leq \omega_{pe}t \leq 25$). The dotted line shows the theoretical dispersion relation of the electron Bernstein wave. (b) The snapshot of the E_x at $\omega_{pe}t = 18$, where the spacial region to obtain the above dispersion relation is marked by the arrow. (c) The dispersion relation for E_z obtained by space-time Fourier transformation ($540 \leq$ x ≤ 796, and $20 \leq \omega_{pe}t \leq 71$). (d) The snapshot of the E_z at $\omega_{pe}t = 66$, where the spacial region to obtain the above dispersion relation is marked by the arrow.

important simulation result on the proton acceleration is that the surfatron acceleration mechanism can operate only in the propagation angles between 90 and 70 degree.

Next we investigate the nature of the electrostatic waves excited behind the shock. Fig.3 shows dispersion relation and spatial distribution of both E_x and E_z for model (1). Fig.3(b) shows the spatial distribution of E_x at $\omega_{pe}t = 18$. We can see small oscillations behind the shock. To understand the characteristics of the electrostatic field behind the shock, we perform two-dimensional Fourier transformation: one-space and one-time for first 512 steps ($\omega_{pe}t = 0$ to $\omega_{pe}t = 25.6$) and $x = 70$ to $x = 326$ (the region is shown by the arrow in Fig.3(b)). Then we obtained the dispersion relation of the electrostatic waves, as shown in Fig.3(a). The excited waves are shown by solid contour lines. The black dot line shows the theoretical curve of the electron Bernstein mode, which theoretical curve is obtained from the following dispersion equation (Stix 1992),

$$1 - \frac{2\omega_{pe}^2}{\lambda\omega_{ce}^2} e^{-\lambda} I_1(\lambda) \frac{\omega_{ce}^2}{\omega^2 - \omega_{ce}^2} = 0 \qquad (1)$$

where I_1 is the modified Bessel function of the first order, and $\lambda = k^2 v_{th,e}^2/\omega_{ce}^2$. The electron Bernstein mode is defined by the parameters with the high density plasma where the Bernstein mode is excited: $\omega_{ce}/\omega'_{pe} = 0.63$ and $v_{th,e}/c = 0.1$. Here ω_{pe} and ω'_{pe} are the plasma frequency in the low density and high density plasma, respectively. The frequency ratio of them is 2.0. The frequency and wave number in the dispersion relation are normalized by ω_{pe} and ω_{pe}/c respectively, where ω_{pe} is defined by using the electron density in the low density region. As seen in Fig.3(a), we conclude that the excited electrostatic waves are the electron Bernstein mode that may be generated by counter-streaming electrons behind the shock.

Fig.3(d) shows a snapshot of the electric field E_z at $\omega_{pe}t = 66$. As seen in Fig.3(d) (the region shown by an arrow), we find that the extra-ordinary electromagnetic waves (X-mode) are emitted from the shock front. To obtain the dispersion relation of the emitted X-mode, we perform two-dimensional Fourier transformation: one-space and one-time for $\omega_{pe}t = 20$ to $\omega_{pe}t = 71$ and $x = 540$ to $x = 796$ (the region is shown by the arrow in Fig.3(d)). Then we obtained the dispersion relation of the X-mode, as seen in Fig.3(c). The frequency of the emitted X-mode is in the range between $1.4\omega_{pe}$ and about $3.5\omega_{pe}$. The emission mechanism of the X-mode is due to the direct linear mode conversion (Budden 1961) from the electron Bernstein mode due to the density gradient near the shock front.

Next we add external magnetic field B_x and we in-

vestigate the effect of oblique propagation of shocks on the wave emission from the shock front. We changed the propagation angle from 90 degree to 40 degree. The electromagnetic wave emission was observed in the above angles. Here we present the simulation result for the propagation angle of 80 degree (Model(2)). Fig.4 shows dispersion relation and spatial distribution of both E_x and E_z for model (2). Fig.4(b) shows the spatial distribution of E_x at $\omega_{pe}t = 18$. We can see small oscillations behind the shock. To understand the characteristics of the electrostatic field behind the shock, we perform two-dimensional Fourier transformation: one-space and one-time for first 512 steps ($\omega_{pe}t = 0$ to $\omega_{pe}t = 25$) and $x = 70$ to $x = 326$ (the region is shown by the arrow in Fig.4(b)). Then we obtained the dispersion relation of the electrostatic waves, as shown in Fig.4(a). The excited waves are shown by solid contour lines. The black dot line shows the theoretical curve of the obliquely propagating Langmuir wave (Z-mode) , which theoretical curve is obtained from the following dispersion equation,

$$\omega^2 = {\omega_{pe}}^2 + 3k^2{v_{th,e}}^2 + \omega_{ce}^2 sin^2\theta \qquad (2)$$

where $v_{th,e}$ is the electron thermal velocity and θ is the angle between the wave-vector and the magnetic field. We used $v_{th,e} = 0.1c$ and $\theta = 4\pi/9$. As seen in Fig.4(a), we conclude that the excited electrostatic waves are the Z-mode that may be generated by counter-streaming electrons behind the shock.

Fig.4(d) shows a snapshot of the electric field E_z at $\omega_{pe}t = 66$. As seen in Fig.4(d) (the region shown by an arrow), we find that the extra-ordinary electromagnetic waves (X-mode) are emitted from the shock front. To obtain the dispersion relation of the emitted X-mode, we perform two-dimensional Fourier transformation: one-space and one-time for $\omega_{pe}t = 20$ to $\omega_{pe}t = 71$ and $x = 540$ to $x = 796$ (the region is shown by the arrow in Fig.4(d)). Then we obtained the dispersion relation of the X-mode, as seen in Fig.4(c). The frequency of the emitted X-mode is in the range between $1.4\omega_{pe}$ and about $3.2\omega_{pe}$. The emission mechanism of the X-mode is due to the direct linear mode conversion from the Z-mode due to the density gradient near the shock front.

To see the timing of emission of fundamental and second harmonic, we present the time history of E_z for Model (1)(in Fig.5(a)), and Model (2)(in Fig.5(b)), that are obtained from the Inverse Fourier transformation using the data of Fig.3(c) and Fig.4(c), respectively. The solid line showing the fundamental emission is obtained by using data of $1.5 \leq \omega/\omega_{pe} \leq 2.0$ and $0 \leq kc/\omega_{pe} \leq 3.0$, and the dashed line showing the second harmonic is obtained by using data of $2.5 \leq \omega/\omega_{pe} \leq 3.5$ and $0 \leq kc/\omega_{pe} \leq$

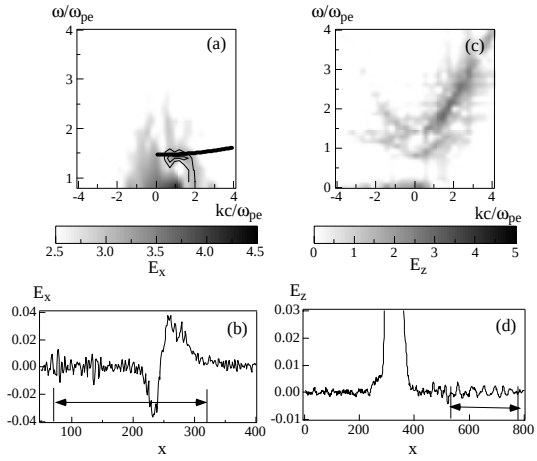

Figure 4: Simulation results for Model (2): (a) The dispersion relation for E_x obtained by space-time Fourier transformation ($70 \leq$ x ≤ 326, and $0 \leq \omega_{pe}t \leq 25$). The dotted line shows the theoretical dispersion relation of the Langmuir wave (z-mode). (b) The snapshot of the E_x at $\omega_{pe}t = 18$, where the spacial region to obtain the above dispersion relation is marked by the arrow. (c) The dispersion relation for E_z obtained by space-time Fourier transformation ($540 \leq$ x ≤ 796, and $20 \leq \omega_{pe}t \leq 71$). (d) The snapshot of the E_z at $\omega_{pe}t = 66$, where the spacial region to obtain the above dispersion relation is marked by the arrow.

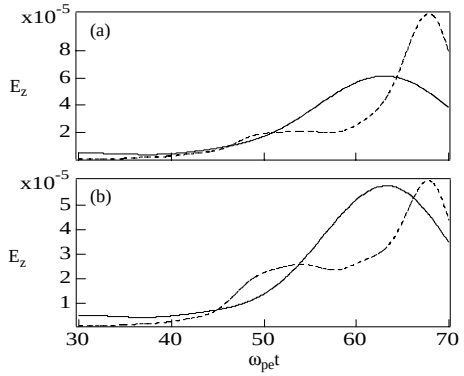

Figure 5: Time history of E_z for Model (1)-(a), and Model (2)-(b), that are obtained from the Inverse Fourier transformation using the data of Fig.3(c) and Fig.4(c). The solid line is obtained by using data of $1.5 \leq \omega/\omega_{pe} \leq 2.0$ and $0 \leq kc/\omega_{pe} \leq 3.0$, and the dashed line is obtained by using data of $2.5 \leq \omega/\omega_{pe} \leq 3.5$ and $0 \leq kc/\omega_{pe} \leq 4.0$.

4.0. As seen in Fig.5, the second harmonic emission is slightly delayed from the fundamental emission for both cases.

From other simulation results in which we changed the shock propagation angle from 90 to 40 degree, we conclude that the Z-mode can be excited with the amplitude as the same as the case presented here and therefore the extra-ordinary electromagnetic waves are also emitted from the shock front as the same way presented here. The details of the simulation results of other angles will be published elsewhere.

4 Summary

We investigated the wave emission process of solar Type II radio bursts associated with Coronal Mass Ejections (CME) by using two dimensional, electromagnetic, relativistic Particle-In-Cell (PIC) code. We performed two simulations : the first case is that the CME propagates perpendicular to the local magnetic field, and the second case is that the CME propagates obliquely to the local magnetic field where only the case of the propagation angle of 80 degree is shown. It was shown that fast magnetosonic shock wave is formed with both protons and electrons accelerated by the surfatron acceleration mechanism. It was also shown from the first case that near the shock front the electron Bernstein waves are generated and they can be converted to the extra-ordinary electromagnetic waves (Type II radio bursts) through the direct linear mode conversion. It was found from the second case that near the shock front the electrostatic Langmuir waves (Z-mode) are generated and they can be also converted to the extra-ordinary electromagnetic waves through the direct linear mode conversion.

5 Acknowledgments

S. Saito is supported by research fellowship of the Japan Society for the Promotion of Science (JSPS) for young scientists, as JSPS Research Fellow.

References

[1] Aschwanden, M. J. 2004, in Physics of The Solar Corona, Springer-Verlag, Chap.15, 657

[2] Budden, K. G. 1961, Radio Waves in the Ionosphere, Cambridge Univ. Press, New York.

[3] Buneman, O. 1993, in Computer Space Plasma Physics, Simulation Techniques and Software, edited by Matsumoto, H. & Omura, Y. Terra Scientific, Tokyo, p.67

[4] Cairns, I. H., Knock, S. A., Robinson P. A. & Kuncic Z. 2003 Space Sci. Rev., 107(1-2), 27

[5] Cliver, E. W. Webb D F., & Howard, R. A. 1999, Sol Phys. 187, 89

[6] Goldman, M. V. & Smith, D. F. 1986, Chap. 15 in Physics of the SUN, Vol. 2 edited by P.A. Sturrock, T.E. Holzer D. M. Mihalas and R K. Ulrich, D. Reidel Publ. Co., p.325

[7] Melrose, D. B. 1980, Aust. J. Phys., 33, 121

[8] Ohsawa, Y. 1985, Phys. Fluids, 28, 2130

[9] Ohsawa, Y., & Sakai, J. I. 1987, ApJ., 313, 440

[10] Sakai, J. I. & Ohsawa, Y. 1987, Space Sci. Rev. 46, 113

[11] Simnett, G. M. 2003, Sol. Phys., 213, 387

[12] Simnett, G M. 1, Sakai J I. & Forsyth, R J. 2003, A & A., submitted

[13] Smith D. F. 1970, Adv. Astro. Astrophys. 7, 147

[14] Stix, T H. 1992, Waves in Plasmas (New York: AIP)